Journal of Materials Chemistry

Cite this: *J. Mater. Chem.*, 2012, **22**, 21928

www.rsc.org/materials

PAPER

Heterogeneous nucleation of protein crystals using nanoporous gold nucleants

F. Kertis,†[a] S. Khurshid,†[b] O. Okman,[c] J. W. Kysar,[c] L. Govada,[b] N. Chayen*[b] and J. Erlebacher*[a]

Received 11th July 2012, Accepted 31st August 2012
DOI: 10.1039/c2jm34527g

We present a theory and experiments that help clarify the origin of the effectiveness of nanoporous substrates in the heterogeneous nucleation of protein crystals. The central idea tested here is that when a substrate (or "nucleant") possesses pores of the order of the hydrodynamical radius of a protein, then the entropic penalty associated with nucleating a protein crystal on that surface may be alleviated. Model experiments using lysozyme and nanoporous gold (NPG) substrates suggest that there is indeed a reduction in the entropy associated with creating critical nuclei, but the magnitude of the reduction is small. Taken together with further examination of protein crystallization with NPG nucleants using four other proteins, our aggregate results suggest that surface chemistry and surface area effects play the dominant role in nucleation when using these nanoporous nucleants.

1. Introduction

In a typical protein crystallization experiment, good quality crystals suitable for X-ray diffraction structure determination may be found by constructing an empirical phase diagram that indicates when protein becomes supersaturated as the background concentration of a precipitant is increased, as discussed in ref. 1 and schematically illustrated in Fig. 1. With the use of such a phase diagram, a typical protein crystallization trial proceeds by setting a droplet containing a slightly unsaturated solution of protein and a buffer, and letting this droplet equilibrate against a reservoir solution containing a precipitant at a higher concentration. This precipitant concentration difference drives water to evaporate from the protein solution and condense in the reservoir, ultimately supersaturating the protein and driving crystal nucleation and growth. Usually by the time the protein nucleates out of solution, it is quite supersaturated, and allows identification of a "metastable zone" on the protein crystallization phase diagram through which the protein solution passes before significant numbers of crystals appear. Good nucleation, *i.e.*, with just a few defect-free crystals forming, is found by driving the solution only slightly out of the metastable zone, so that when nucleation does occur, the remaining solution drops in protein concentration and allows growth to occur without new crystals forming.

A recent trend in protein crystallization has been the introduction of secondary, chemically inert materials into the protein solution as "nucleants" that induce the heterogeneous nucleation of protein crystals.[2] More specifically, it has been found that when the nucleant has the form of a nanoporous material with a pore diameter of similar order of magnitude as the protein molecule (hydrodynamical) diameter, then nucleation of protein crystals occurs at milder supersaturation conditions than usual, leading to higher quality crystals. Such heterogeneous nucleation suggests a lower energy barrier for nucleation, and in this paper we explore this concept in quantitative detail by using a model nanoporous nucleant, nanoporous gold (NPG), made by electrochemical dealloying. NPG is a nearly pure gold material made

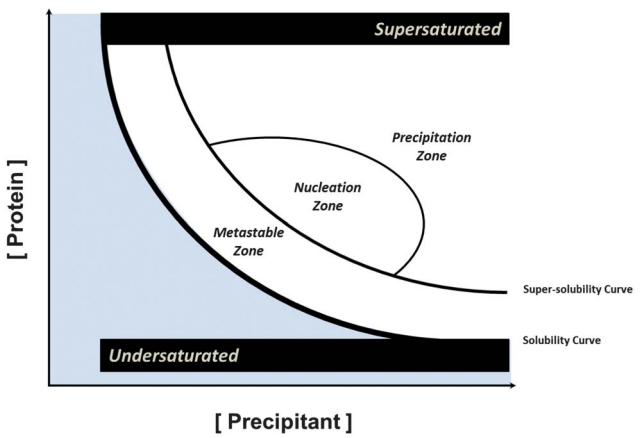

Fig. 1 Typical protein crystallization phase diagram, showing regions of undersaturation and supersaturation. A strategy for good protein crystallization is to drive nucleation to occur at protein and precipitant concentrations corresponding to the intermediate metastable zone; further into the nucleation zone, more crystals are formed, and they are often of lower quality.

[a]*Department of Materials Science and Engineering, Johns Hopkins University, Baltimore, MD 21218, USA. E-mail: jonah.erlebacher@jhu.edu*
[b]*Biomolecular Medicine, Department of Surgery and Cancer, Faculty of Medicine, Imperial College London, Sir Alexander Fleming Building, London SW7 2AZ, UK. E-mail: n.chayen@imperial.ac.uk*
[c]*Department of Mechanical Engineering, Columbia University, New York, NY 10027, USA*
† These authors contributed equally to the manuscript.

by electrochemical dissolution of silver from silver/gold alloys, a process that results in the re-organization of the gold atoms to form a three-dimensional bi-continuous porous metal with ligament and pore sizes tunable from 5 nm to many microns.[3,4]

Theoretical models have been introduced to explain the facile nucleation of proteins on porous substrates. van Meel *et al.*[5] suggest that proteins nucleate on porous substrates by first undergoing capillary condensation into pores at which point they nucleate; further microscopic roughness helps by keeping any nucleus from strongly adsorbing to the surface, an effect that would lead to strain within the crystal and stymie growth; this idea refines the earlier notion of Page and Sear[6] who suggested that geometric "corner" features in porous substrates can lead to facile protein nucleation. In both cases, these analyses have assumed the protein to be homogeneous particles whose internal degrees of freedom (*e.g.*, entropy of water solvation, entropy of vibrational and configurational modes) make negligible contributions to the work required to form the critical nucleus.

Is it a good approximation to ignore entropic effects in protein nucleation on nanoporous substrates? Empirical evidence suggests that there is something special about the pore size being of the order of the size of the protein being crystallized that leads to more facile crystallization. This observation suggests that a cluster of protein molecules might lodge in a pore in a kinetic pathway to form a critical nucleus, but be able to maintain their high entropy because there is a water reservoir underneath them. The relative entropy of crystallization of a protein crystal nucleated on a nanoporous substrate compared to a planar one can be measured by finding the nucleation rate I as a function of temperature T. This follows simply from classical nucleation theory, which may be applied to protein crystallization as long as one is careful not to make assumptions about enthalpic and entropic contributions to the free energy of nucleation.[7] The nucleation rate is the number of nuclei appearing in the parent phase per unit time per volume (for homogeneous nucleation) or per area (for heterogeneous nucleation). Classical nucleation theory yields the following form for the nucleation rate, I:[8]

$$I = A\exp\left(-\frac{Q_D}{k_B T}\right)\exp\left(-\frac{\Delta G_{crit}}{k_B T}\right). \quad (1)$$

Here, Q_D is an activation barrier for the protein to transfer from the solution to the nucleus, and the free energy ΔG_{crit} is work required to create a nucleus with a critical radius. The constant A is an amalgamation of various terms: the number of sites available for a nucleus to start forming, the jump frequency, the interfacial energy between the protein crystal and solution, and a geometric factor accounting for a jump in the right direction. Writing $\Delta G_{crit} = \Delta H_{crit} - T\Delta S_{crit}$, the nucleation rate *versus* temperature takes the simple form:

$$I = A\exp\left(-\frac{(Q_D + \Delta H_{crit})}{k_B T}\right)\exp\left(\frac{\Delta S_{crit}}{k_B}\right). \quad (2)$$

Here, k_B is Boltzmann's constant and T is temperature. It is reasonable that ΔH_{crit}, Q_D, and A will be nearly the same for heterogeneous nucleation on planar and nanoporous substrates made of the same material. The ratio of nucleation rate on a nanoporous (np) substrate I_{np} to a planar (pl) one I_{pl} will be

$$\frac{I_{np}}{I_{pl}} = \frac{A_{np}}{A_{pl}}\exp\left(\frac{\Delta S_{crit,np} - \Delta S_{crit,pl}}{k_B}\right). \quad (3)$$

This is a very sensitive ratio: With the assumption that $\Delta S_{crit} \sim -0.002$ eV K^{-1} molecule (see below), then for equal substrate surface areas A_{pl} and A_{np}, if $\Delta S_{crit,np} \sim 0.9\Delta S_{crit,pl}$, the nucleation rate should be increased by over a factor of 10 under the same temperature and supersaturation conditions.

In this study, protein crystallization was studied using nanoporous gold nucleants in a variety of form factors. To examine the validity of eqn (3), we report a quantitative study of the heterogeneous nucleation rate of lysozyme on planar substrates in the sitting drop configuration, a globular protein roughly ellipsoid in shape whose major axis has a diameter of 5.5 nm and its minor axis is roughly 3.3 nm,[9] and for which the thermodynamics of nucleation at room temperature have been well-measured. Through measuring the temperature dependency of its solubility, the enthalpy and entropy of crystallization of lysozyme were found to be $\Delta H_m \sim -0.7$ eV per molecule and $\Delta S_m \sim -0.002$ eV K^{-1} molecule (including water) respectively; so the value of free energy of crystallization is only $\Delta G_m \sim -0.06$ eV per molecule at 298 K,[10] only ~2 to 3 times higher than $k_B T$ (note that here we use the subscript 'm' to signify a per molecule basis, not a per mole basis). Vekilov and Yau estimated the surface energy to be $\gamma \sim 0.57$ mJ m^{-2},[11] and with these numbers the critical radius $r_c = -2\gamma/\Delta G_V$ is estimated to be between 1 and 10 nm. That is, the critical nucleus is comprised of about 2–10 molecules considering that the radius of many proteins is ~5 to 10 nm. This agrees with atomic force microscopy studies and nucleation rate studies[11] that also directly suggest that the critical radius is comprised of only 2–10 molecules. This size is directly comparable to the pore diameter in nanoporous gold, motivating its use as a nucleant. In addition to the planar substrate studies, hanging drop crystallization trials were performed using nanoporous gold flakes as nucleants, in which the pore size, dealloying conditions, and surface chemistry of the flakes were modified to examine nucleation and crystal growth of a variety of different proteins.

2. Experimental

2.1 Nanoporous gold nucleants

For sitting drop experiments to quantitatively measure the nucleation rate, foils of composition $Ag_{65}Au_{35}$ were patterned with circular regions of NPG with 5 mm diameter by dealloying the material locally through a PDMS mask. The electrolyte used to dealloy these regions was 0.1 M $AgNO_3$ at 0.55 V. Foils were prepared according to the recipe in,[3] and the dealloying conditions are discussed in ref. 12. Dealloying in a neutral solution instead of an acid, which is more common, avoids penetration of the electrolyte laterally under the mask and keeps the edges of the patterned region sharp. This dealloying method also ensures formation of small pores, of the order of 10 nm diameter. Fig. 2 shows a representative example of a patterned region of NPG. Patterned samples were also prepared galvanostatically, using methods described in ref. 13, yielding essentially identical behavior. For hanging drop crystallization trials using different model proteins, powders of NPG were prepared by free

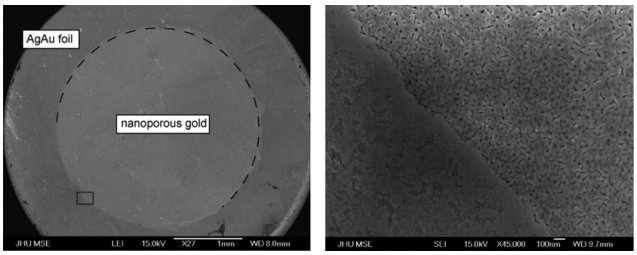

Fig. 2 Scanning electron microscopy (SEM) images of patterned nanoporous gold. (Left): a low-resolution micrograph showing the circular region of patterned nanoporous gold on a large, undealloyed Ag–Au foil. (Right): higher-magnification micrograph showing the distinct interface between the undealloyed Ag–Au foil and the circular region of NPG. In this sample, the foil was annealed for a short time in order to coarsen the pores and increase contrast. No preferential nucleation was observed at the edge of the NPG region.

corrosion of $Ag_{65}Au_{35}$ in nitric acid, which were then rinsed and crumbled into powder.

2.2 Sitting drop experiments

Crystallization experiments upon patterned NPG and dense gold controls were performed in the sitting drop configuration within a custom crystallization chamber made of Teflon with a borosilicate glass cover. The volume of the reservoir solution was 3 mL and the volume of the crystallization droplet was 2.5 μL. Protein and salt (sodium chloride) concentrations were set to 40 mg mL^{-1} and 5% (w/v), respectively; these values are within the metastable region of the lysozyme protein phase diagram[14] and confirmed in our laboratory. A challenge found was that variations in temperature during the course of a crystallization experiment, even of 1 to 2 degrees, significantly altered the nucleation rate of lysozyme. This issue was surmounted by using a thermoelectric heating/cooling plate controllable to between −20 °C and 100 °C, on which we place an insulating chamber with circulating airflow. A schematic of the crystallization plate that was placed within this chamber is shown in Fig. 3. In this way, the temperature of the experiment was controlled and remained constant to within 0.1 °C over the course of any one experiment. Three different temperatures were explored: 23.0 °C, 25.0 °C, and 29.0 °C. At higher temperatures, lysozyme remained soluble, and at lower temperatures, nucleation either occurred too slowly or the protein came out of solution in a non-crystalline form.

To measure the nucleation rate, images were made of the patterned NPG region of the surface on which the protein solution sat and crystals were counted to find the number appearing per unit time. A microscope and a digital camera suspended on a boom arm over the experiment took time-lapse photos of the experiment. Photos were taken once a minute, with $t = 0$ corresponding to the time the experimental chamber is sealed and the crystallization droplet begins to equilibrate with the reservoir. Once a set of photos were taken, they were compared and analyzed using image processing software (Photoshop and ImageJ). To count crystals, from an image with crystals was digitally subtracted an earlier image from the same region, one without crystals. Other than enhancing contrast and brightness to make the edges of the crystals more distinct, there was no further manipulation of the original photo. Because each patterned region is of the same area, the number of crystals appearing per area per unit time was found by counting. Images separated by some amount of time (usually 10 to 20 minutes) were subtracted from one another and the contrast adjusted so that the crystals were easier to see.

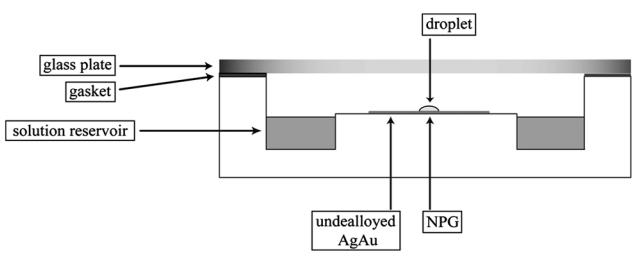

Fig. 3 Sitting drop experimental configuration showing a schematic cross-section of the crystallization chamber. The salt solution reservoir, the sample placement, and the borosilicate top plate with silicone gasket are illustrated.

2.3 Crystallization with NPG nucleants

Crystallization trials utilizing NPG flake nucleants were performed in a hanging drop vapour diffusion format. Nextal™ (Qiagen) plates were employed as standard as were crystallization droplet volumes of 2 μL and reservoir volumes of 500 μL. The samples were incubated at 20 °C. Model proteins tested (the structures of which are well defined at high resolution) included lysozyme from chicken egg white (Sigma, L6876), thaumatin from *Thaumatococcus danielli* (Sigma, T7638), trypsin from bovine pancreas (Sigma, T4665) and haemoglobin from bovine blood (Sigma, H2500). The target protein tested was myosin binding protein C (MyBPC, human c0–c1 domain provided by the Redwood group, Oxford University).

Working phase diagrams were determined for each protein by dispensing one protein concentration against an incremental range of precipitant concentrations. Drop phenomena were observed daily. After a period of one week, NPG nucleants were added to the crystallization drops which remained clear. These

Table 1 The various NPG samples tested and their respective pore sizes. Generation 2 represents the initial move towards 'powder' NPGs. Generation 3 NPGs were of fixed pore size, 25–30 nm, and functionalized by coating with alkanethiols, mercapto-carboxylic acids or an amine-reactive cross linker

Generation 1	
NPG1	5–10 nm
NPG2	~20 nm
NPG3	~50 nm
Generation 2	
NPG1	5–10 nm
NPG2	15–20 nm
NPG3	25–30 nm
NPG4	30–35 nm
NPG5	45–50 nm
NPG6	~55 nm
Generation 3	
NPG1	1-Octanethiol
NPG2	1-Hexadecanethiol
NPG3	8-Mercaptooctanoic acid
NPG4	16-Mercaptohexadecanoic acid
NPG5	Dithiobis succinimidyl propionate

Table 2 List of the proteins tested and the crystallization conditions to which the NPG nucleants were introduced

Protein	Conc. (mg mL^{-1})	Crystallization conditions
Lysozyme	20	1.5–3.0% w/v sodium chloride, 0.1 M sodium acetate, pH 4.5
Thaumatin	30	0.2–0.5 M sodium potassium tartrate, 0.1 M bis-trispropane, pH 6.8
Trypsin	60	12–15% w/v PEG 8k, 0.2 M ammonium sulphate, 0.1 M sodium cacodylate, pH 6.5
Haemoglobin	60	20–23% w/v PEG 3350, 0.2 M magnesium chloride, 0.1 M Bis-Tris, pH 5.5
MyBPC	14	13–15% w/v PEG 3350, 0.1 M HEPES, pH 6.8

drops correspond to the region immediately below the supersolubility curve of the phase diagram. This was done using forceps, ensuring addition of as small a fragment of NPG as possible. Control drops without the presence of nucleants were also prepared for each trial. Table 1 lists the NPG nucleant samples studied and Table 2 details the crystallization conditions for each protein trial. Three form factors ("generations") of NPG were used: "Generation 1" NPG prepared by dealloying in a neutral solution was a soft foil which had to be torn to an adequate size; "generation 2" 'powder' NPG was prepared by free corrosion in concentrated nitric acid and rinsed in pure water; "generation 3" 'powder' NPG was prepared first by free corrosion in concentrated nitric acid, rinsed in water, incubated in an ethanoic solution of the listed thiols, and rinsed in water again. The addition of alkanethiols increases the hydrophobicity of the NPG surface, while the addition of DPS as a surface layer to NPG introduces a surface chemistry that binds to primary amines on the nucleating protein. NPG pore sizes in all cases were controlled by short anneals in air at 400 °C.

3. Results and discussion

3.1 Sitting drop experiments

Fig. 4 shows two representative datasets from the sitting drop experiments. Each trial, whether on NPG or dense Au, showed four distinct regimes which we label as (1) induction/equilibration, (2) transient nucleation, (3) steady state nucleation, and (4) depletion. During induction/equilibration, the sitting drop equilibrates against the reservoir solution and becomes supersaturated; there are no nuclei visible through the light microscope. The appearance of the first visible nuclei marks the start of the transient nucleation regime. In this time period critical nuclei form, remain stable within the solution and continue to grow, but the rate at which they appear has not yet reached a steady state. After some time, the experiment reaches steady state nucleation in which new crystals appear at a linear rate. Eventually, no new crystals form and the existing protein crystals just continue to grow.

We observed a distinct difference in the timescales for each of the regimes for NPG compared to dense Au substrates under otherwise equivalent conditions. At 23.0 °C lysozyme crystals were first visible at 135 minutes while they first appeared at 80 minutes on NPG. The same trend was seen at 25.0 °C and

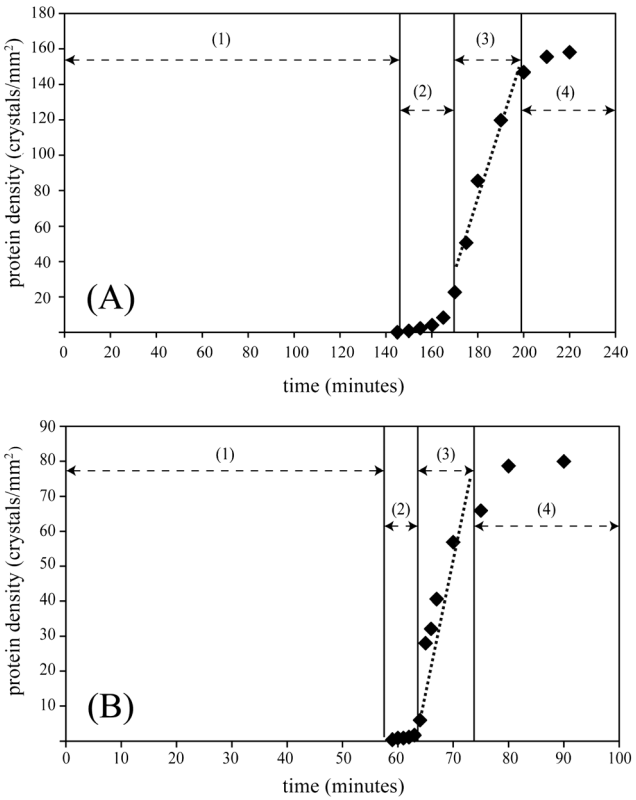

Fig. 4 Representative data from crystallization trials over (A) dense Au and (B) NPG; 5% NaCl, 40 mg mL^{-1} lysozyme, 23 °C; data for protein density are shown as black diamonds. Each experiment showed four characteristic regions: (1) induction, (2) transient nucleation, (3) steady-state nucleation (regressions are shown as dotted lines), and (4) growth. Use of NPG significantly reduced the induction time as well as the overall number of crystals, reflecting the significantly higher supersaturation achieved without NPG.

29.0 °C, where it would take a little over two hours for crystals to appear over dense Au and only 90 minutes for droplets sitting on NPG. In addition, the transient nucleation regime was much longer for runs on dense Au than on NPG, as well as the overall timespan of the steady state regime.

Fig. 5 shows data for the natural logarithm of the steady state nucleation rate over NPG plotted *versus* $1/k_BT$, where each point represents the average of three crystallization trials. As T increases, the nucleation rate decreases, indicating the expected decrease in supersaturation as temperature increases. The slope of $\ln(I)$ *vs.* $1/T$, from eqn (2), is $(\Delta H_{crit} + Q_D)/k_B$, for which we find the value $\Delta H_{crit} + Q_D \sim 1.4$ eV per molecule, a reasonable value of the order of the (absolute value of the) enthalpy of crystallization for lysozyme, discussed above.[10]

Although our crystallization rates on planar gold substrates are similar, our best data, with the smallest error bars, are at 296 K. At this temperature, the average nucleation rate was 12.6 crystals per cm^2 per s over NPG, while over dense Au the same conditions resulted in an average nucleation rate of 7.3 crystals per cm^2 per s. To use eqn (3) to back out the difference in the entropy of nucleation on a porous substrate and a planar substrate, we need to know the area of the protein solution in contact with NPG (A_{np}) and the planar substrate control (A_{pl}), respectively. The value of A_{np} is not the total geometric area of

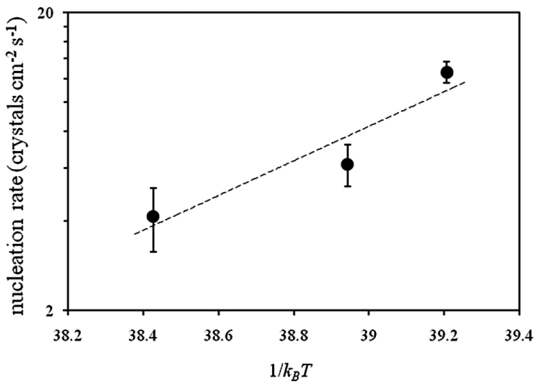

Fig. 5 Nucleation rate of lysozyme on nanoporous gold *vs.* $1/k_BT$.

the porous region, including the surface area of all internal pores, because the physical dimensions of the pores should limit diffusion of protein at any substantial distance within the pores. The roughness factor of NPG (the ratio of surface area to projected surface area) is ~10 for every 100 nm of depth of porosity, and samples here were dealloyed to approximately that depth. Thus, we estimate that the range of (A_{pl}/A_{np}) is less than 1.0 and greater than 0.1. Using eqn (3), which uses the ratio of nucleation rates, we find a range for $\Delta S_{crit,np} - \Delta S_{crit,pl}$ between 4.7×10^{-5} eV per (K molecule) and 2.4×10^{-4} eV per (K molecule). At $T = 296$ K, this results in a difference in the contribution to the free energy of nucleation, $T(\Delta S_{crit,np} - \Delta S_{crit,pl})$, of between 0.01 eV per molecule and 0.07 eV per molecule. Even on assuming an unphysically large roughness factor of 100, this contribution only rises to 0.13 eV per molecule, a value still significantly smaller than the enthalpic contribution $\Delta H_{crit} + Q_D \sim 1.4$ eV per molecule discussed earlier.

3.2 Hanging drop experiments

Generation 1 and 2 NPG nucleants prompted nucleation at metastable conditions for lysozyme, thaumatin, trypsin and MyBPC. The resulting crystals were large and single, with growth occurring from the NPG surface; examples are clearly shown in Fig. 6. The respective control drops remained clear. Furthermore, NPG induced crystal growth was reproducible with crystals of similar size and number appearing in repeats. Generation 2 'powder' NPG nucleants proved to be the most potent, reproducibly facilitating nucleation at lower precipitant concentrations (deeper into the metastable region).

Handling of the nucleants was straightforward (comparing favourably to other known nucleants such as porous silicon, horse hair and bio-glass). They also allowed easy visualization and scoring due to their well-defined edges. Summary results for each protein at metastable conditions (where the corresponding control drops remained clear) are as follows:

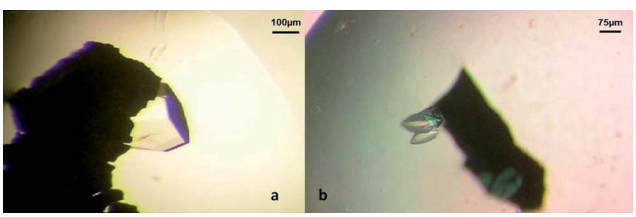

Fig. 6 (a) A lysozyme crystal growing from the surface of a 20 nm pore-size NPG nucleant sample and (b) spear shaped MyBPC crystals growing from the surface of a 50 nm NPG sample. Both crystallization trials were performed under metastable conditions.

Lysozyme. Crystal formation was observed at the metastable cusp (3% sodium chloride) for each of the NPG samples with the exception of the ~50 and ~55 nm samples. Further into the metastable region (2 and 2.5%), the 20 nm NPG was the only sample to reproducibly induce nucleation (8/10 trials with Generation 1 NPG and 10/10 trials with Generation 2 NPG).

Trypsin. At the metastable cusp (15% ammonium sulphate), all samples with a pore size greater than 30 nm gave rise to crystals. Further into the metastable region (13 and 14%), only the ~20, 25–30 and 30–35 nm samples were successful. At 13% ammonium sulphate, crystals were observed in 7/10 trials with Generation 1 NPG at ~20 nm. The corresponding value for the Generation 2 sample at 25–30 nm was 9/10 trials.

Thaumatin. All samples gave rise to crystals at the metastable cusp (0.5 M sodium potassium tartrate). Further into the metastable region (0.35, 0.4 and 0.45 M), samples with pore diameters ranging between 5 and 30 nm were successful inducers of crystal nucleation. The ~20 nm and 25–30 nm samples proved most potent (8/10 trials with both Generation 1 and 2 NPGs at 0.4 M sodium potassium tartrate).

Haemoglobin. No crystals were observed with any of the samples. This protein undergoes 'Ostwald ripening' whereby crystals grow from a precipitate which forms first. In this case the gold colour of the nucleant is hard to distinguish against the red colour of the precipitate formed.

Human cardiac myosin binding protein/C (MyBPC). Crystal growth was prompted at 14 and 15% PEG 3350 using NPG with pores at ~20 and ~50 nm. This was observed in 9/10 trials for the latter and 8/10 trials for the former (both Generation 1 samples).

Generation 3 NPGs. Fig. 7 illustrates the ability of the functionalized NPGs to prompt crystal formation under metastable conditions for each of the model proteins tested (including haemoglobin). This phenomenon, however, was not reproducible. In the case of lysozyme for example, each of the five samples yielded crystals, albeit in a combined 9/25 trials. The same can be said for 8/25 trypsin trials (only NPGs 3 and 4), 4/25 thaumatin trials (NPG2 only) and 3/25 haemoglobin trials (NPG3 only). The results clearly indicate that the surface coatings interfered with the nucleating ability of these nucleants. Nucleant texture was also influenced with each of the samples disintegrating upon slight probing with forceps. Consequently, their insertion into crystallization drops became troublesome with multiple fragments being introduced unwillingly. This resulted in excessive nucleation events, explaining the observation of heavy precipitates in a large number of trials.

Taken together, the crystallization trials using the different proteins (lysozyme (14.5 kiloDalton, kD), thaumatin (22 kD), trypsin (24 kD), haemoglobin (64.5 kD), MyBPC (12 kD)) and the different NPG nucleants form a broad survey of different

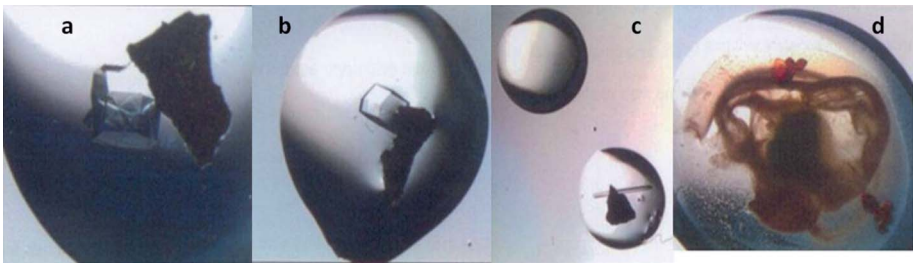

Fig. 7 Metastable crystallization drops containing generation 3 "functionalized" NPGs. (a and b) Large, single lysozyme crystals growing from NPG3 and NPG2 respectively. (c) A large single trypsin crystal growing from NPG4 and a clear control drop. (d) Haemoglobin crystals growing from NPG3, partially obscured by its characteristic precipitate.

molecular weight proteins and different surface functionalizations. The question we were attempting to answer with the survey of proteins was the following: while we saw that for lysozyme, a surface area increase led to "better" nucleation, is this a universal phenomenon? Does surface area increase always lead to better crystallization kinetics? There is clearly a lower bound – 5 nm pore NPG generally led to bad crystallization, perhaps due to steric inhibition of proteins entering the pores. Compared to lysozyme, slightly larger proteins such as trypsin and thaumatin (24 kD) nucleated well on porous gold with slightly larger pore sizes (30 nm *vs.* 20 nm). But haemoglobin did not crystallize with any nucleant, and we are unable at this point to identify any clear trend.

General observations. To succinctly summarize our results, the sitting drop experiments show that the entropic contribution to the free energy of crystallization of lysozyme using NPG nucleants is small; as such, dramatic changes to the surface chemistry and surface area should lead to large changes in crystallization behavior, and this has been demonstrated with the hanging drop experiments. Decreases in the pore size increased the ratio A_{pl}/A_{np}, leading to more facile crystallization within the metastable region. And changes in the surface energy with the addition of the various thiol-terminated molecules examined also led to changes in the nucleation behavior.

Our results here suggest that the hypothesis that protein crystallization on nanoporous gold nucleants is substantially driven by reductions in the entropy of forming the critical nucleus is incorrect, and lends credence to the approximation found in theoretical considerations of proteins as colloidal spheres. The "lock and key" model proposed by Chayen *et al.*,[15] essentially a completely enthalpic model, remains the most viable for protein nucleation. The observations of shorter incubation times and transient nucleation periods must also be considered in light of this result. It is likely that these observations are due to capillary effects associated with nanoporous gold, *i.e.*, their higher surface area and high curvature pores allow them to more quickly equilibrate with their environment, in this case the salt reservoir. Such speedy equilibration has been observed using NPG in other contexts such as capillary wetting.[16]

4. Conclusions

A study using nanoporous gold as a substrate or nucleant for the heterogeneous nucleation of protein crystals was performed. The results demonstrate the relatively small importance of entropic contributions to the free energy of crystallization compared to the enthalpic interaction between the particular protein to be crystallized and the nucleant surface. This observation should help guide future studies of nanoporous nucleants for protein crystallization by highlighting the importance of tailoring favorable energetic interactions between the protein and the substrate. Although such engineering presumes some information about the external chemical moieties of the protein (*e.g.*, might they contain exposed cysteines that can bind to gold), it is likely that crystallization trials will be greatly benefitted by such an approach.

Acknowledgements

The authors are grateful to the US National Science Foundation and the UK Engineering and Physical Sciences Research Council *via* a Materials World Network program funded under grants DMR-0804187 (NSF) and EP/G027005 (EPSRC).

References

1 N. E. Chayen, Methods for separating nucleation and growth in protein crystallization, *Prog. Biophys. Mol. Biol.*, 2005, **88**, 329–337.
2 E. Saridakis and N. E. Chayen, Towards a 'universal' nucleant for protein crystallization, *Trends Biotechnol.*, 2009, **27**, 99–106.
3 F. Kertis, J. Snyder, L. Govada, S. Khurshid, N. Chayen and J. Erlebacher, Structure–processing relationships in the fabrication of nanoporous gold, *JOM*, 2010, **62**, 50–56.
4 S. Van Petegem, S. Brandstetter, R. Maass, A. M. Hodge, B. S. El-Dasher, J. Biener, B. Schmitt, C. Borca and H. Van Swygenhoven, On the microstructure of nanoporous gold: an X-ray diffraction study, *Nano Lett.*, 2009, **9**, 1158–1163.
5 J. A. van Meel, R. P. Sear and D. Frenkel, Design principles for broad-spectrum protein-crystal nucleants with nanoscale pits, *Phys. Rev. Lett.*, 2010, **105**, 205501.
6 A. J. Page and R. P. Sear, Heterogeneous nucleation in and out of pores, *Phys. Rev. Lett.*, 2006, **97**, 065701.
7 O. Galkin and P. Vekilov, Are nucleation kinetics of protein crystals similar to those of liquid droplets?, *J. Am. Chem. Soc.*, 2000, **122**, 156–163.
8 D. T. Wu, *Nucleation Theory, Solid State Physics*, ed. H. Ehrenreich and F. Spaepen, Academic Press, San Diego, 1997, vol. 50, pp. 37–187.
9 J. D. Gunton, A. Shiryayev and D. L. Pagan, *Protein Condensation: Kinetic Pathways to Crystallization and Disease*, Cambridge University Press, Cambridge 2007.
10 P. G. Vekilov, A. R. Feeling-Taylor, S.-T. Yau and D. Petsev, Solvent entropy contribution to the free energy of protein crystallization, *Acta Crystallogr., Sect. D: Biol. Crystallogr.*, 2002, **58**, 1611–1616.

11 S.-T. Yau and P. Vekilov, Quasi-planar nucleus structure in apoferritin crystallization, *Nature*, 2000, **406**, 494–497.
12 J. Snyder, K. Livi and J. Erlebacher, Dealloying silver/gold alloys in neutral silver nitrate solutions: porosity evolution, surface composition, and surface oxides, *J. Electrochem. Soc.*, 2008, **155**, 464.
13 O. Okman and J. W. Kysar, Fabrication of crack-free blanket nanoporous gold thin films by galvanostatic dealloying, *J. Alloys Compd.*, 2011, **509**, 6374–6381.
14 E. Cacioppo and M. L. Pusey, The solubility of tetragonal form of hen egg white lysozyme from pH 4.0 to 5.4, *J. Cryst. Growth*, 1991, **114**, 286–292.
15 N. E. Chayen, E. Saridakis and R. P. Sear, Experiment and theory for heterogeneous nucleation of protein crystals in a porous medium, *Proc. Natl. Acad. Sci. U. S. A.*, 2006, **103**, 597–601.
16 E. Seker, M. R. Begley, M. L. Reed and M. Utz, Kinetics of capillary wetting in nanoporous films in the presence of surface evaporation, *Appl. Phys. Lett.*, 2008, **92**, 013128.

